Supramolecular Mimic for Bottlebrush Polymers in Bulk

Golkaram, Milad; Boetje, Laura; Dong, Jingjin; Aguilar Suarez, Luis; Fodor, Csaba; Maniar, Dina; van Ruymbeke, Evelyne; Faraji, Shirin; Portale, Giuseppe; Loos, Katja

Published in:
ACS Omega

DOI:
10.1021/acsomega.9b02126

Publication date:
2019

ACS OMEGA

Article

Cite This: ACS Omega 2019, 4, 16481−16492

http://pubs.acs.org/journal/acsodf

Supramolecular Mimic for Bottlebrush Polymers in Bulk

Milad Golkaram,[†] Laura Boetje,[†] Jingjin Dong,[†] Luis Enrique Aguilar Suarez,[‡] Csaba Fodor,[†,∥] Dina Maniar,[†] Evelyne van Ruymbeke,[§] Shirin Faraji,[‡] Giuseppe Portale,[†] and Katja Loos*[,†]

[†]Macromolecular Chemistry and New Polymeric Materials, Zernike Institute for Advanced Materials and [‡]Theoretical Chemistry Group, Zernike Institute for Advanced Materials, University of Groningen, Nijenborgh 4, 9747 AG Groningen, The Netherlands

[§]Bio- and Soft Matter, Institute of Condensed Matter and Nanosciences, Université Catholique de Louvain, Croix du Sud 1, B-1348 Louvain-la-Neuve, Belgium

Supporting Information

ABSTRACT: A series of poly(tetrahydrofuran)s with molecular weights above entanglement molecular weight M_e were synthesized, and one of their end-groups was functionalized with a supramolecular entity so that the corresponding polymers form a brushlike structure suitable for comparison with conventional irreversible bottlebrush polymers. To compare their relaxation mechanisms, linear rheology was employed and showed that a hierarchical relaxation, which is usually observed in bottlebrush polymers, occurs in these materials, too. The polymer chain segments close to the supramolecular backbone are highly immobilized due to strong association in the center of polymer brush and cannot relax via reptation mechanism, which is mainly responsible for linear entangled polymer relaxations. Therefore, disentanglement can take much longer through contour length fluctuations and arm retraction processes similar to covalent bottlebrush polymers and combs. The relaxed ends of polymers then act as solvent to let the remaining segments of the polymeric brush undergo Rouse-like motions (constraint release Rouse). At longer times, additional plateau appears, which can be attributed to the relaxation of the entire supramolecular bottlebrush polymer via hopping or reptative motions. With an increase of temperature, viscoelastic solid behavior turns into viscoelastic liquid due to reversible depolymerization of the supramolecular backbone of the bottlebrush polymer. The elastic modulus (G' in the order of kPa) was much less than the values found for the entanglement plateau modulus of linear poly(tetrahydrofuran) (in order of MPa). This low modulus value, which exists up to very low frequencies (high temperatures), makes them a good candidate for supersoft elastomers.

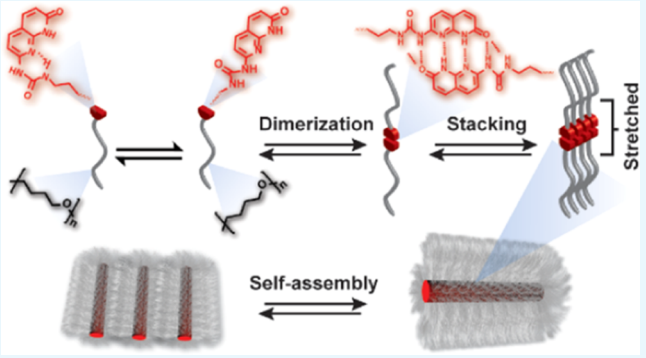

INTRODUCTION

The rheological properties of polymers are governed by dynamics at the molecular level. By introducing topological constrains to the polymeric chains, relaxation mechanism within different segments of the chains in different time scales can be altered. Vlassopoulos,[1−4] McLeish,[5−10] and Larson[11,12] extensively studied brush/comb/star polymer dynamics. The dynamics of these systems are generally described by a hierarchical relaxation process, in which the segments furthest from the backbone relax first while the internal segments near branch points relax at later times within a solvated tube.[13]

The main interest concerning star polymers is the topological constraint they "feel" in the melt state. By changing the length and number of arms, bulk properties can vary from a typical linear polymer to colloidal materials.[3,14,15] When the length of the polymers is large enough, the topological constraints of the surrounding chains (entanglement) confine a chain within a so-called tube.[16] On the other hand, if the number of arms is high enough (hyperstars), the star polymers can behave as colloidal hard spheres which are constrained by their neighbors and form a glasslike material in the sense that they are not ordered (nor cross-linked) but do not flow. These materials are totally a different class of polymers compared to glassy polymers whose glass-transition temperature prevents them from flowing at certain temperatures. In this system, the topological constraint is the cage of surrounding particles that limits the motion of each star to scales smaller than its size, and therefore no macroscopic motion can be observed.[3,14,15]

In this study, we investigate the effect of additional dynamic feature, namely, association/dissociation of multiple H-bonding groups (sticker), in the dynamics of polymer brushes. The only study on polymer combs with noncovalent main-chain/side-chain interactions used thymine/diaminotriazine moieties randomly distributed along the main chain.[17−19] However, the disadvantages of this system are: (1) random distribution of junction points, which can affect the relaxation

Received: July 10, 2019
Accepted: September 10, 2019
Published: September 25, 2019

Scheme 1. Synthesis and End-Group Modification of Poly(tetrahydrofuran) (1) Using H-Bonding Moiety (2)

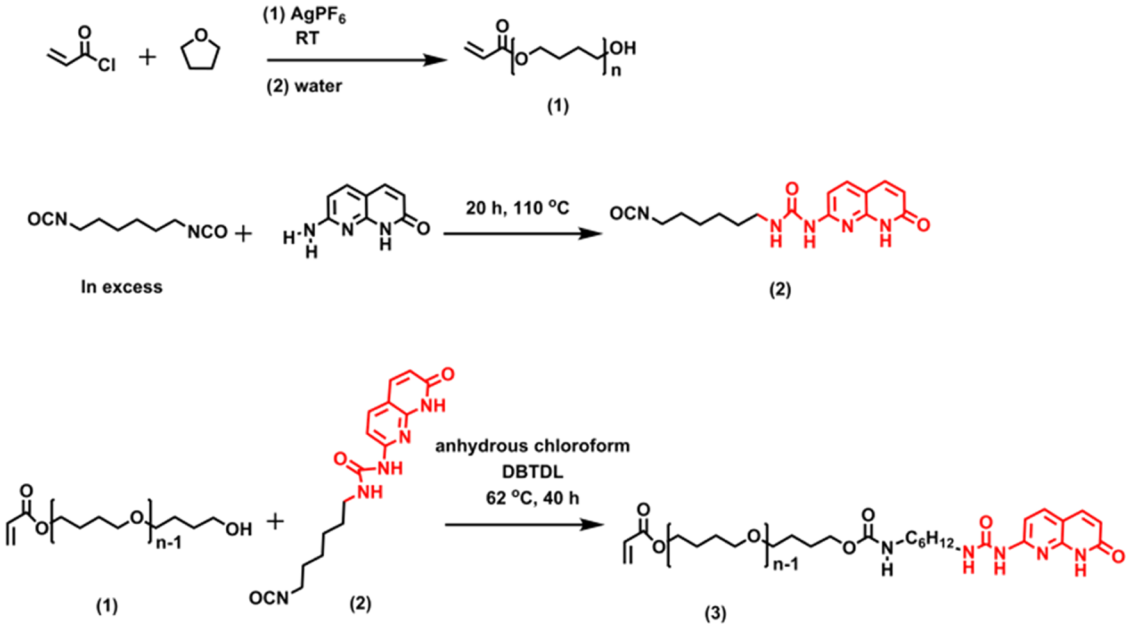

of supramolecular polymers via broader relaxation times, (2) weak H-bonding, which does not have a long lifetime, (3) the fact that despite heteroassociation of thymine and diaminotriazine moieties, the homoassociation and aggregations can be significant,[20] and (4) using few stickers along the chain, only a comb morphology can be obtained, whereas to deviate from linear polymer dynamics, more side chains are more effective for a hierarchical relaxation. But for more side chains to associate (to compete with the steric hindrance), a sticker capable of strong stacking/H-bonding is needed. Therefore, to tackle these problems, a novel sticker was synthesized and added to one end of a model polymer with low critical molecular weight M_c (=2500 g mol^{-1})[21] so it can be highly entangled while having low molecular weight (important for end-group functionalization) and with medium polarity so that sticker dynamics can be incorporated in entangled polymer dynamics in a brushlike fashion. It is important to note that in this study, the goal was to investigate an entangled polymer with one sticker as the end-group. The presence of two stickers or more can lead to the formation of transient networks that have entirely different viscoelastic properties, which has been studied extensively in the past.[22−24]

RESULTS AND DISCUSSION

Synthesis of Poly(tetrahydrofuran)s (PTHFs) (1a−d). Synthesis of different molecular weights of PTHFs (**1a−d**) having only one hydroxyl group was inspired by the works of Croucher, Thompson, and co-workers.[25−27] Silver tetrafluoroborate ($AgBF_4$) or equivalently silver hexafluorophosphate ($AgPF_6$) can be used as a catalyst, and when added to acryloyl chloride can generate a cationic initiator. The initiation rate depends on the precipitation rate of the formed AgCl and in all cases was less than 30 s at room temperature, leading to a fast initiation suitable for living polymerization. Gram-scale synthesis can be carried out to yield PTHFs with high molecular weights and narrow dispersity (Scheme 1 and Table 1). The gel permeation chromatography (GPC) traces (Figure S1) show four different PTHF molecular weights proving that the synthesized polymers have low-molecular-weight distributions. ^{1}H NMR proves the successful formation of PTHF (**1a−d**) bearing one hydroxyl group originating from quenching with water and the other end bearing the acrylate from the initiator (Figure S2). PTHF was used due to its low glass-transition temperature ($T_g \approx -86$ °C)[22,28] and fast dynamics above melting point ($T_m \approx 30$ °C, Figure S11) in the range of the studied molecular weights (≫critical molecular weight $M_c \approx 2500$ g mol^{-1}).[21] The medium polarity of PTHF is also particularly interesting as even weak H-bonding moieties (weak stickers) can associate strongly in a nonpolar matrix like polyisobutylene.[29]

Table 1. Molecular Characterization of Supramolecular Polymers

entry	sample	M_n[a] (kg mol^{-1})	$Đ$[a]	Z[b]
1	**3a**	11.0	1.10	9
2	**3b**	14.5	1.02	12
3	**3c**	30.1	1.17	24
4	**3d**	35.0	1.23	28

[a]Calculated via GPC measurements. [b]Number of entanglements calculated based on M_c = 2500 g mol^{-1} for linear PTHF.[21]

Also, we investigated the polymerizability of acrylate end-group and no conversion occurred, proving that the functionality stays intact due to steric hindrance and low concentration of end-groups in such molecular weights. In the future, new methods will be reported on how to polymerize this end-group to form bottlebrush polymers with stickers at the free ends.

Self-Assembly Studies. To introduce end-groups that can efficiently self-assemble, both the strength of the sticker and more importantly its ability to undergo phase segregation are proved to be crucial.[22] To obtain an array of associated end-groups resembling a backbone of polymer brushes, the goal is more than just a binary association of stickers; long-range, well-defined association as well as aggregation has to be achieved. Therefore, we decided to synthesize a sticker that can self-assemble in large scales using six H-bondings, two of which are bifurcated. Moreover, the aromatic ring(s) can undergo $\pi-\pi$

DOI: 10.1021/acsomega.9b02126
ACS Omega 2019, 4, 16481−16492

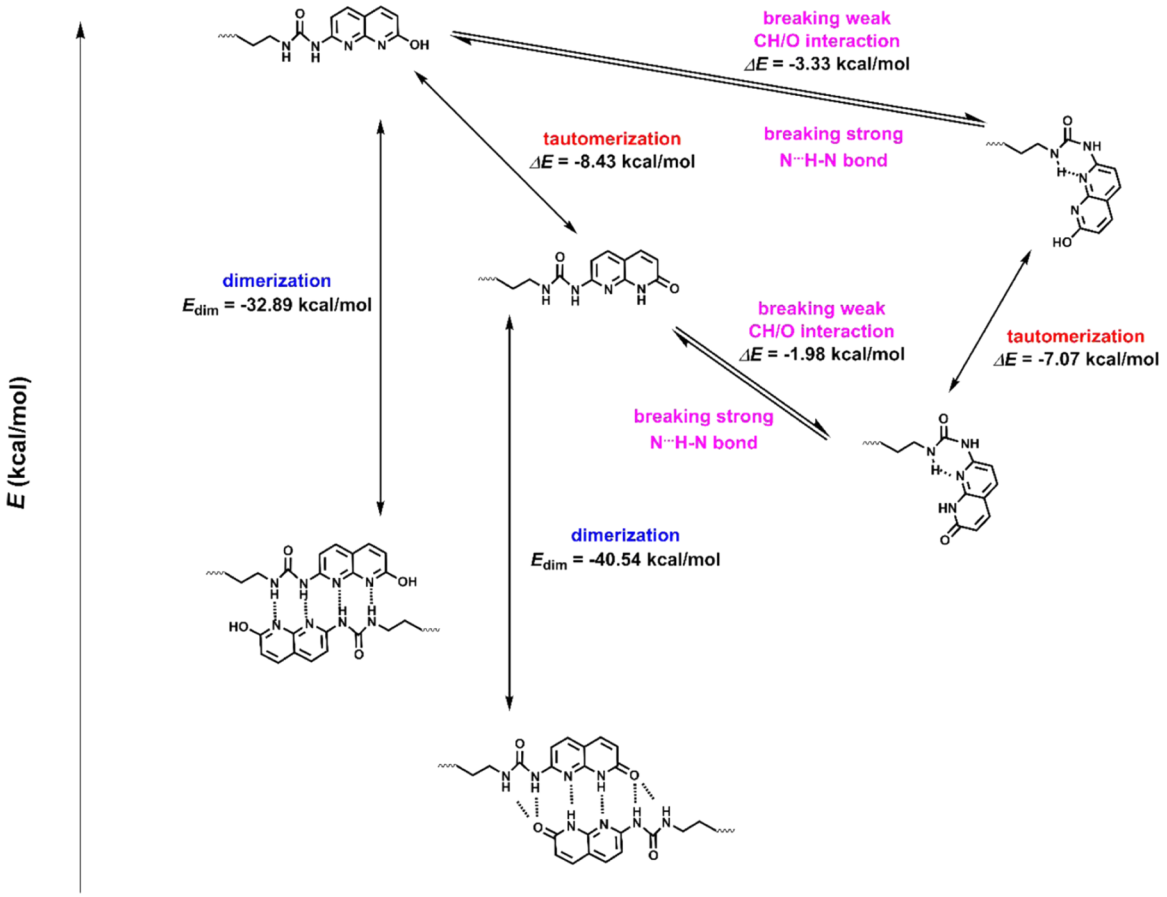

Figure 1. Energy diagram for **2** [polarizable continuum model (PCM), chloroform] showing tautomerization, intramolecular H-bonding formation, and dimerization energies. Energy (stability) levels decrease (increase) from top to bottom.

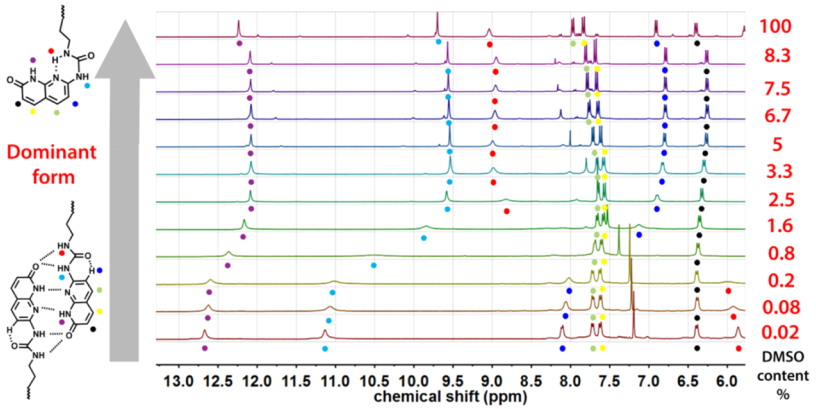

Figure 2. ^{1}H NMR titration of **2** in chloroform-*d* with DMSO-d_6 as the guest compound.

stacking, which can help the long-range aggregation of stickers. The trivial, gram-scale synthesis of compound **2** (1-(6-Isocyanatohexyl)-3-(7-oxo-7,8-dihydro-1,8-naphthyridin-2-yl)-urea) (**ODIN**) makes it a strong candidate for supramolecular chemistry (compound **2** in Scheme 1). The most remarkable character of this sticker compared to the well-known ureido-pyrimidinone (UPy) is its better phase separation ability that induces long-ranged stacked layers needed for a brush backbone, whereas UPy without a urea group attached to it only partially aggregates, as will be discussed in detail in this article.[30] However, the association of **ODIN** is not necessarily trivial, as it is the case for many H-bonding systems in which urea groups are involved.[31−34] A few primary mechanistic questions can be raised concerning the designed sticker: (i) can the heterocyclic urea be folded by an intramolecular H-bonding? (ii) if so, how can it affect the association and dimerization? (iii) which tautomeric form is more stable (Figure 1)? (iv) how can this sticker influence the properties of a model polymer in the melt state when attached to only one end of the polymeric chain? In the following, we strive to provide convincing answers to these questions.

Sticker **2** was coupled to one end-group of PTHFs **1a−d** so that the association can be studied in a polymeric system. Figures S3 and S4 depict the ^{1}H NMR spectra of **2** and **3**,

DOI: 10.1021/acsomega.9b02126
ACS Omega 2019, 4, 16481−16492

respectively. The downfield chemical shift of protons adjacent to the hydroxyl group of **1** as well as appearance of protons corresponding to **2** proves the addition of the sticker to one end-group of the PTHF. Moreover, the broad urethane proton at 4.76 ppm substantiates the coupling. The degree of coupling is calculated roughly to be around 70% (depending on which proton is considered), which is satisfactory for such high PTHF molecular weights (>11.0 kg mol^{-1}).

To answer the first question, ^{1}H NMR was used to check whether breaking of intermolecular H-bonding using a strong hydrogen-bond acceptor such as dimethyl sulfoxide (DMSO) can isolate the stickers from a dimerized state in chloroform (Figure 2). In a very low ratio of DMSO/chloroform, the ^{1}H NMR (only the downfield section of the spectra is illustrated) shows two protons at very high ppm values (>11 ppm). This indicates that the aromatic N−H (proton assigned with purple) and urea proton adjacent to the aromatic ring (light blue) are involved in strong H-bondings. The third proton (red) is however shifted relatively upfield. The four aromatic peaks are all duplets, and the coupling constants prove the correct assignment of these protons. By increasing the DMSO content to only 0.08%, an upfield shift in the strongly hydrogen-bonded protons (assigned with purple and light blue) arises. Moreover, these peaks broaden and at 0.8% DMSO, all NH protons are coalesced, indicating the equilibrium between the monomeric and dimeric forms of **2** in the NMR timescale.

However, more interesting is the upfield shift and coalescence of the aromatic proton adjacent to the urea carbonyl (dark blue). This shows that **2** in its dimeric form has a weak C−H···O═C hydrogen bond that can solidify the conformational form (Figure 1) and prevent it from rotating to create the forms with intramolecular N−H···N H-bonding. Although this effect is relatively weak, intermolecular or intramolecular H-bonding of C−H···N/O has been reported earlier.[34,35] The change in the chemical shift (8.19−6.83 ppm) of the aromatic proton in the proximity of O═C (dark blue) is also induced due to an anisotropic deshielding cone of O═C in full agreement with similar heterocyclic ureas.[33,34,36] This interaction is more probable in the case of the hydrogen-bonded dimer in which rotation is limited due to six hydrogen bonds with the other monomer. Therefore, when the intermolecular H-bonding is broken, the rotation occurs implying that in the monomeric form, keto tautomer is more stable, whereas the keto dimer is a stable conformation when the two stickers are in close proximity to each other, in nonpolar solvents or the melt state. In the keto monomer, the formed six-membered ring is strongly rigid, creating three six-membered rings adjacent to each other. The very strong intramolecular H-bonding formed in the keto monomer is also observable from deshielding of the urea proton (noted with red color) from 5.93 to 8.98 ppm. This peak was coalesced in the intermediate concentrations of DMSO (0.08−2.5%) indicating the "pathway" to the corresponding the keto monomer conformation while being in equilibrium with the monomeric form with no intramolecular N−H···N H-bonding. Moreover, the sharpening and appearance of a weak triplet (Figure S5) indicates the coupling of N−H (red) and adjacent CH_2 protons in the formed rigid structure and that the N−H proton (red) is not in equilibrium or exchange with other molecules. This phenomenon does not occur in the intermolecularly hydrogen-bonded protons as a broad singlet can be seen (^{1}H NMR in pure chloroform, Figure S3). Moreover, by increasing the DMSO contents, three of the aromatic protons (green, yellow, and black) have a slight upfield shift, showing the $\pi-\pi$ stacking is broken by the presence of DMSO molecules. They also start to sharpen with addition of DMSO, which shows that the broadness of the aromatic peaks can originate from stacking.[37] The trend in the upfield shift for the protons is indicated by green and yellow but stops at 6.7% DMSO probably due to the countereffect of intramolecular H-bonding formation. The slight shift of the spectrum when comparing 8.3−100% DMSO concentrations is due to the electric field and magnetic anisotropy of DMSO as a solvent, which affects all protons equally.[38]

At higher concentrations of DMSO, some traces of other conformers are also present. From the two very weak peaks at 10−12 ppm, they can be assigned to keto monomer with no intramolecular N−H···N H-bonding. Also, the aromatic protons exist at 6.4−8.2 ppm. Using the aromatic protons for the integration, roughly 20% of this conformer is still present in pure DMSO. To summarize, the keto monomer with intramolecular H-bonding is built via first breaking the intermolecular hydrogen bond and the $\pi-\pi$ stacking and then breaking the weak intramolecular C−H···O═C hydrogen bond and the subsequent rotation to form a stronger N−H···N bond.

The stability of the formed H-bonding depends on many factors including the strength and the number of intermolecular hydrogen bonds,[39] secondary interactions (SIs),[40] steric effects, and competition with solvent molecules.[41] Also, according to Etter's rules, intramolecular H-bonding is generally stronger than the intermolecular one.[42] For sticker **2**, if the weak intramolecular C−H···O═C interaction is ignored, the number of strong intermolecular hydrogen bonds in the dimer is rather high (6). Moreover, the SIs can play an important role in the association as in the DDADAA array, N:O and N:N are repulsive. This is in fact consistent with the calculated dimerization constant ($K_{dim} \approx 20\,000$ M^{-1}) of this moiety in chloroform. Unfortunately, due to the low solubility of this compound, accurate dilution experiments were not possible; therefore, K_{dim} was measured after coupling to the PTHF chain end according to the previously reported ^{1}H NMR integration method of Meijer et al. and using the aromatic proton (dark blue), which can form weak H-bonding over any other aromatic integrals (see Supporting Information).[43] This value is fairly consistent with the values reported for similar stickers ($K_{dim} \approx 40\,000$ M^{-1}).[44] Therefore, the violation of Etter's rule (six intermolecular H-bonding is preferred over one intramolecular one) occurs with the expense of dimerization constant.[34]

So far, ^{1}H NMR showed the presence of dominantly keto forms. However, the absence of enol monomer and dimer is still dubious. To have a deeper insight into the stability in different conformers, electronic structure calculations at the density functional level of theory, density functional theory (DFT) (omega B97X-D functional/cc-PVDZ basis set), was used to evaluate the molecular structures, dimerization energies (E_{dim}), and the energetics of different conformers. Calculations were conducted in both vacuum and chloroform using polarizable continuum model (PCM).

Figure 1 shows the energy profiles and corresponding structures of different tautomers (the stability increases from top to bottom). Enol monomer appeared to be the least stable one and tends to tautomerize into the keto form. Even formation of an internal H-bond and a six-membered ring does

DOI: 10.1021/acsomega.9b02126
ACS Omega 2019, 4, 16481−16492

not suffice to induce much stability to this conformer. A DDAA-type interaction, which is also responsible for UPy association, is not the most favorable interaction, even though it has a high energy of dimerization (E_{dim} = −32.89 kcal mol^{-1}). The calculated E_{dim} of UPy in the keto form (DDAA) is reported to be −41.76 kcal mol^{-1}.[45] The lower E_{dim} of enol dimer is mainly due to the secondary interaction of the additional hydroxyl group, steric hindrance, and lack of a strong intramolecular H-bonding. This leads to a deviation from the planar geometry and formation of a distorted plane (Figure S6). As stated earlier, ^{1}H NMR showed that the weak C−H···O interaction is partially responsible for the stability of monomeric forms without internal strong H-bondong. Therefore, the energy required to break the intramolecular hydrogen bond of **2** is much smaller than expected (1.98 kcal mol^{-1}). Nevertheless, consistent with ^{1}H NMR, when isolated from other partners, the most stable tautomer is calculated to be the keto monomer. Finally, the dimerization of keto form of **2** leads to a high E_{dim} of −40.54 kcal mol^{-1}, very close to UPy with E_{dim} = −41.76 kcal mol^{-1}. This is also consistent with our ^{1}H NMR analysis showing that in the dimerized form in chloroform (or in vacuum), keto form is the most stable dimer/conformer. This value for similar naphthyridine-based compounds with DADA-type H-bonding was only −16.55 to −23.58 kcal mol^{-1},[36] implying that the bifurcated urea hydrogen bond plays a significant role in the dimerization of **2**.

Although, considering E_{dim}, the H-bonding interaction of UPy·UPy is slightly stronger than **2** (from K_{dim}, it is even more significant), the enthalpy of stacking (the magnitude) is rather much higher in **2** ($E_{stacking}$ = −18.96 kcal mol^{-1}) than in UPy ($E_{stacking}$ = +4 kcal mol^{-1}). Also, keto form of **2** in the dimerized form showed a very planar geometry (Figure 3) as

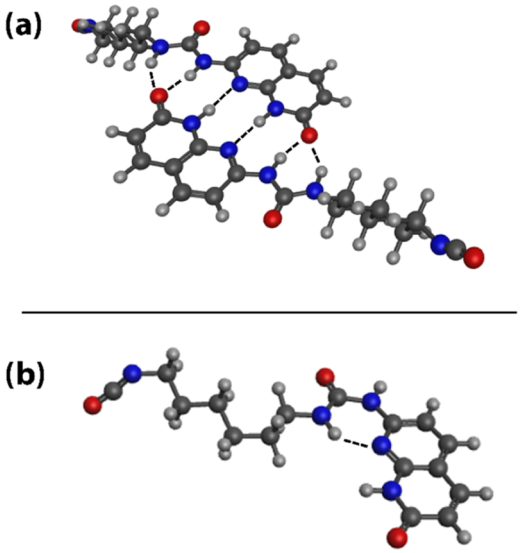

Figure 3. Optimized structures of (a) dimeric and (b) monomeric forms of **2** as the most stable conformers in the dimeric and monomeric states.

opposed to the enol form. However, probably due to the two aromatic rings present in enol, the stacking is slightly stronger ($E_{stacking}$ in the enol form = −19.45 kcal mol^{-1}). The optimized stacked geometries can be seen in Figure S6.

Also, the urea N−H close to the alkyl spacer seems to be pulled out of the stacking plane to form a hydrogen bond with C═O of the stacked partner promoting the $\pi-\pi$ stacking (Figure S6). Therefore, the urea N−H is not only involved in H-bonding in the dimerization but also in the stacking, leading to a three-dimensional ordering. Another reason for the high stacking ability of **2** can be attributed to the intramolecular interactions CH···O, which can extend π-conjugation by incorporating the H and C═O atoms into the rings.[46]

Unfortunately, single-crystal X-ray diffraction (SCXRD) was not possible due to low solubility of **2** preventing single-crystal growth. However, in future work, we plan to improve the solubility by alkyl chain extension to perform both SCXRD and ^{1}H NMR dilution experiments. Therefore, the bond distance and angles were calculated theoretically at the DFT level of theory (Table S1 for calculations in chloroform and vacuum). Interestingly, the bifurcated hydrogen bonds do not have similar bond lengths (3.02 vs 2.78 Å). This has been reported earlier in the case of dibutyltriurets[47] and is consistent with the ^{1}H NMR assignments (Figure 2). The N−H bond close to the alkyl spacer appears at much lower chemical shifts (5.93 ppm) than the one close to the aromatic rings (11.22 ppm), showing that the strength of urea N−H H-bonding adjacent to the rings is much higher and therefore prone to intramolecular hydrogen bonds with bond length 2.74 Å if it is isolated from its partner (see Figure 3). The weak hydrogen bond in C−H···O is although relatively long (2.87 Å compared to 2.74 Å in the monomeric meto form) still short enough (<3 Å) to stabilize this tautomer via intramolecular interaction. The other two N−H···N bonds in the center of ADADAD, on the other hand, appear to have short bond lengths of 3.07 Å. The estimated values for UPy are 2.78−3.01 Å from ref 38 and 2.75−2.97 Å from our calculations showing the hydrogen-bond length in UPy·UPy is comparable to that of dimer of **2** (2.78−3.07 Å). Also, the bond angles in the two middle N−H···N were calculated to be 176° in comparison to 178° for the two in UPy. Stacking distance for **2** was calculated to be 3.15 Å, which is quite smaller than the one for UPy (3.56 Å) in ref 38. Using powder X-ray diffraction (PXRD) (Figure S13), the stacking distance was calculated to be $d_{\pi-\pi}$ = 3.49 Å, which is again smaller than the UPy stacking distance measured by XRD (3.55 Å).[45]

To get some insight into the association of **2** in the solid state, variable-temperature Fourier transform infrared (VT-FTIR) spectroscopy was performed (Figure 4). The peaks at 2280 and 2800−3000 cm^{-1} belong to the isocyanate and alkyl groups, respectively. The absence of any peaks above 3400

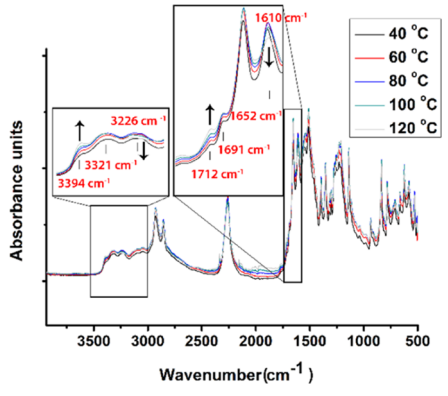

Figure 4. VT-IR of **2** while heated stepwise from 40 to 120 °C with 15 min equilibration time at each temperature.

DOI: 10.1021/acsomega.9b02126
ACS Omega 2019, 4, 16481−16492

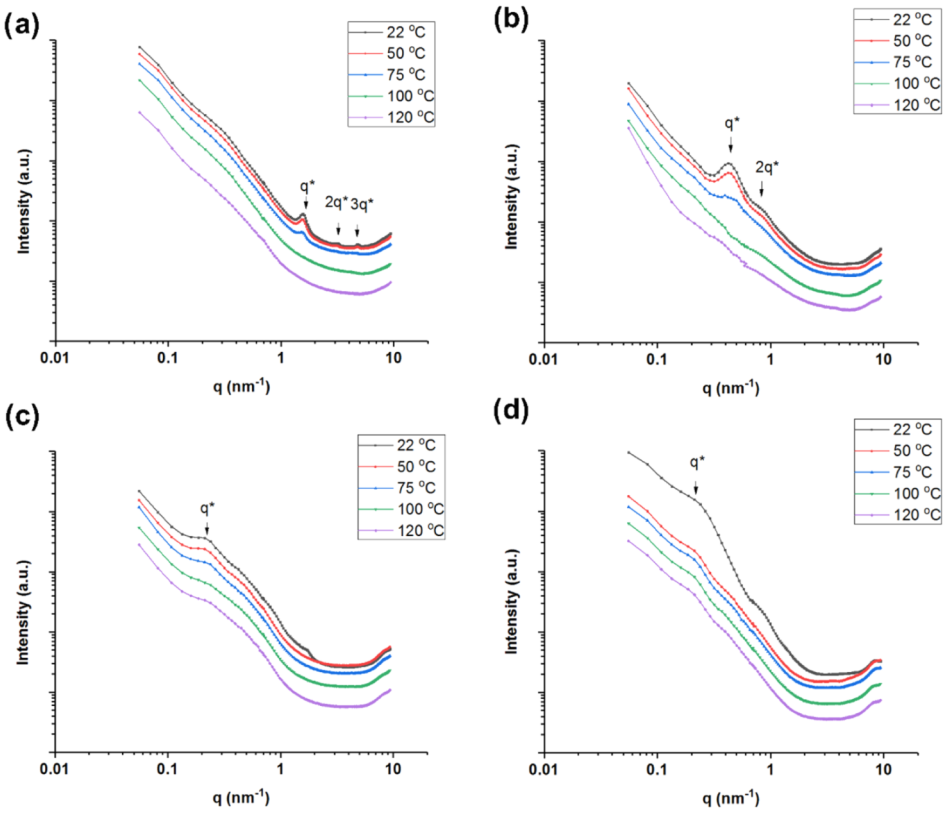

Figure 5. SAXS profiles of supramolecular polymers (a) **3a**, (b) **3b**, (c) **3c**, and (d) **3d** in the melt state at temperatures 22, 50, 75, 100, and 120 °C.

cm^{-1} indicates that almost all of the N−H groups are hydrogen-bonded. Moreover, the peaks at 3394, 3321, and 3226 cm^{-1} correspond to the free, disordered hydrogen-bonded, and ordered hydrogen-bonded N−H. The two peaks at lower wavenumbers are especially broad showing that in terms of bond angle and length, a distribution of H-bonding patterns is present. This is another proof of the theoretical simulation results that the H-bonding in **2** is multidirectional. As discussed earlier, the N−H proton is pulled out of the aromatic plane to form another H-bonding N−H···O═C with the stacked partner (Figure S6). Interestingly, the peak at 3394 cm^{-1} gets stronger in intensity by increasing the temperature whereas the peak assigned to the ordered H-bonding (at 3226 cm^{-1}) starts to lose its intensity at 100 °C. At 1610, 1652, and 1712 cm^{-1}, peaks corresponding to the ordered, disordered hydrogen-bonded C═O, and free C═O, respectively, show the same trend with temperature. The peak at 1610 cm^{-1} starts to lose its intensity at 100 °C whereas the one at 1712 cm^{-1} becomes more intense as temperature increases. This shows that at lower temperatures, part of the moieties are ordered, and this ordering gets weaker with temperature, in particular with rise of temperature to 100 °C. Another implication is that H-bonding assists the ordering and stacking of **2**. This is consistent with the observations for UPy that stacking when combined with H-bonding increases E_{dim}.[45] The assignments were also consistent with the plethora of studies done in the past for urea groups.[48−50]

Small-Angle X-ray Scattering (SAXS). The high stacking energy as well as small stacking distance obtained by DFT calculations in conjunction with PXRD measurements indicates that **2** is a strong candidate for supramolecular aggregation of macromonomers. The aggregation behavior of different molecular weights of PTHF with **ODIN** end-group (**3a−d**) was studied by performing SAXS in the bulk phase. Figure 5 shows the SAXS profiles of **3a−d** at different temperatures starting from room temperature up to 120 °C. The samples were kept above T_m after annealing to avoid crystallization of PTHF (see Supporting Information). All investigated samples show clear scattering at small angles, indicative of the presence of aggregates at the nanoscale.

Generally, the SAXS intensity decays in the log−log plots according to a power law of about q^{-2}. Generally, for rodlike or fibrillar structures, a q^{-1} power law is observed. However, bundling and further aggregation usually alters the slope of the SAXS intensity in the log−log plot and can explain the q^{-2} intensity decay. Thus, we assume that H-bonding motif **2** tends to stack due to $\pi-\pi$ stacking to form elongated one-dimensional (1D) structures that tend to assemble side to side (Figure 7). This kind of structure is generally observed for supramolecular UPy systems.[30] The packing between the 1D aggregates side to side is characterized by a characteristic separation distance d^*, which will depend on the molecular weight of the polymer chains attached to the H-bonding motifs.

The scattering profiles of samples **3a** and **3b** show three and two scattering peaks, respectively. Their relative positions at q^*, $2q^*$, and $3q^*$ for **3a** and q^* and $2q^*$ for **3b** suggest a lamellar morphology with periodicity distance $d^* = 2\pi/q^* = 4$ and 14 nm for **3a** and **3b**, respectively. Samples **3c** and **3d** show only a single weak and broad diffraction peak. As mentioned before, increasing molecular weights is expected to cause an increase of d^*. Indeed, the scattering peak position shifts toward lower scattering angles with increasing molecular weight, meaning that d^* becomes larger (Figure S12).

DOI: 10.1021/acsomega.9b02126
ACS Omega 2019, 4, 16481−16492

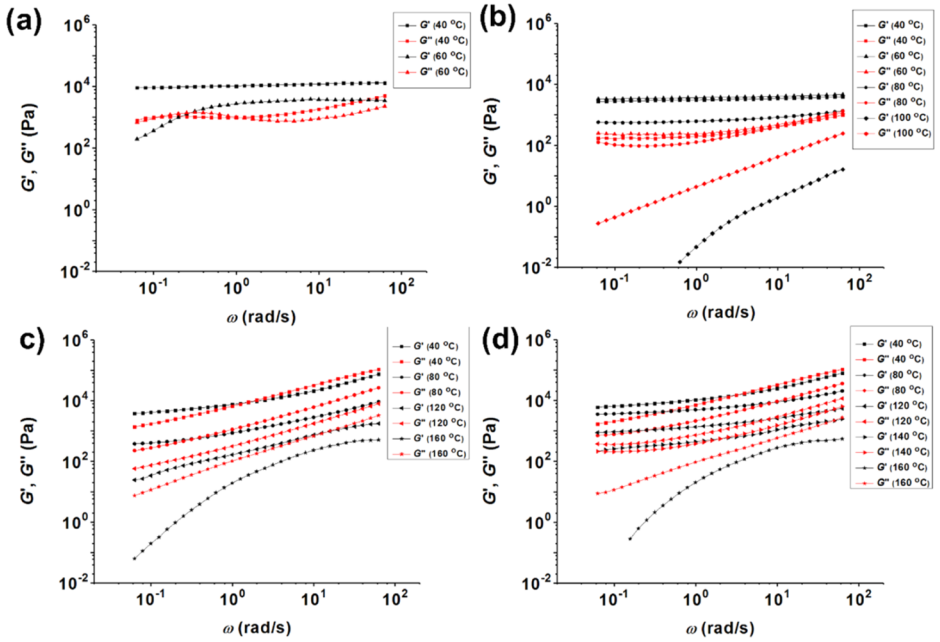

Figure 6. Melt rheology (frequency sweeps) in the linear viscoelastic regime for supramolecular polymers: (a) **3a**, (b) **3b**, (c) **3c**, and (d) **3d** at different temperatures (>40 °C).

However, when plotting d^* as a function of the molecular weight (or the PTHF degree of polymerization), the expected $d^* \propto M_w^{1/2}$ is not observed, and a power exponent of 0.8−1 is found. This would imply a significantly stretched conformation of the polymer chains, a feature that will be discussed below in view of the rheology data.

Furthermore, we have tested the temperature stability of the supramolecular aggregates by performing temperature-resolved SAXS (Figure 5). Increasing the temperature to 75−100 °C causes significant weakening and often disappearance of the scattering peaks for all samples, suggesting loss of molecular order. This temperature range is significantly close to the dissociation temperature estimated by FTIR. However, especially for the two samples with higher molecular weight, the shape of the SAXS curve does not change significantly upon dissociation although scattering features become weaker. This could suggest that even if the H-bonding moieties dissociate, phase separation is still present.

Melt Rheology. To understand the melt dynamics of supramolecular bottlebrush polymers **3a**−**d**, low-amplitude shear rheology was performed in the linear viscoelastic (LVE) regime. Figure 6 shows the frequency sweep measurements performed at different temperatures, starting from 40 °C up to the temperature at which the sample shows viscoelastic liquid behavior or terminal regime; 40 °C was chosen as, at this temperature, all samples are in the noncrystalline phase by differential scanning calorimetry (DSC) measurements (Figure S11). In Figure 6a−d, a significant complex thermorheological behavior prevents the construction of mastercurves. This indicates that the dynamics of **3** is governed by both the association of the end-group and the chain dynamics.[20] Figure 6a shows a plateau with $G' > 10$ kPa at 40 °C, which extends to low frequencies. This behavior is repeated at 60 °C from high to intermediate frequencies, and at longer time, the flow regime appears. At higher temperatures (>80 °C), the viscosity of the sample was too small to be measured accurately. For sample **3b** (see Figure 6b), at low temperatures (40−80 °C), a plateau is also observed ($G' > G''$). At 80 °C, this plateau becomes slightly lower, while at 100 °C, it disappears and a viscoelastic liquid behavior ($G' < G''$) is observed for the whole experimental frequency window. The origin of this plateau is important to be investigated as the reference PTHF polymer **1d** shows liquidlike behavior at all of these temperatures (>40 °C) as $T \gg T_g \approx -86$ °C (Figure S8).[22,28] Therefore, the plateau does not originate from the entanglements and is necessarily due to the contribution of the end-groups aggregation. Besides, comparing to $G_N \approx \rho RT/M_e \approx 1$ MPa in the case of entangled linear PTHF, the observed plateau is much lower. This confirms that a large fraction of the sample has already relaxed at higher frequency outside the experimental frequency window and that this plateau does not correspond to the linear entangled PTHF. It has to be noted that the appearance of a plateau at low frequency cannot be attributed to the formation of a supramolecular network, as often observed with polymer chains carrying supramolecular moieties as their two end-groups[22,23,51] since samples **3a** and **3b** only have one functionalized end-group. Similar behavior was observed for two higher molecular weights **3c** and **3d** in Figure 6c,d (detailed frequency sweeps can be seen in Figures S9 and S10 including all of the studied temperatures). At $T \approx 100$−120 °C, the plateau at low frequencies disappears. Despite the similarities between the two higher and the two lower molecular weights (**3a**/**b** vs **3c**/**d**), there is an important difference to be noted, at intermediate frequencies: for **3c**/**d**, $G', G'' \propto \omega^{0.5}$ for over two decades, while they are constant for **3a**/**b**. Thus, depending on both molecular weight and temperature, three different viscoelastic responses can be observed in the investigated frequency range: (i) a solidlike response ($G' > G''$) observed at low temperatures and often at low frequency; (ii) a dissipative regime observed at high temperatures ($G' < G''$); and (iii) a Rouse regime (with a power law $\sim\omega^{0.5}$) observed at high frequencies for the high-molecular-weight samples.

DOI: 10.1021/acsomega.9b02126
ACS Omega 2019, 4, 16481−16492

To show that the solidlike property arises from aggregation of **2** moieties attached to PTHF, a UPy-modified PTHF using **1d** as precursor was also synthesized (**3e**) (see Supporting Information). The frequency dependence of complex viscosity at 40 °C for **3d** and **3e** is then studied, in comparison to the viscosity of the precursor **1d** and to the one of a low-molecular-weight PTHF bearing hydroxyl end-groups (as a control experiment) (Figure S8). The viscosity of **1d** is over 2 orders of magnitude higher than the low-molecular-weight PTHF. By using UPy, this value increases even more, without increasing the polymer M_n. This increase in viscosity is indicative of a binary association of **2** UPy end-groups leading to a longer PTHF **1d** (around twice the length of **1d**) or to the presence of small aggregates of UPy groups. In this last case, self-assemblies are formed, which relax as starlike molecules (thus, with negligible influence of their small core). It is observed that in all cases except **3d**, a Newtonian, frequency-independent behavior is observed at low frequency, indicating that the terminal regime can be reached for these samples. Moreover, the frequency sweep of **3e** shows a dissipative behavior in the entire frequency range studied (Figure S7). Thus, PTHFs **1** or **3e** are liquidlike materials, despite their entangled state (Table 1), due to temperatures far above their T_g.[22,28] This suggests that UPy, despite stronger dimerization ability, has weaker aggregation and stacking properties than **2**. It can only produce longer chains, almost double size of its precursor **1d** or assemblies obtained by the aggregation of a small number of UPy groups. Samples **3a**−**d**, on the other hand, aggregate much more and form big brushlike objects, which induce an additional rheological response and lead to the presence of the low-frequency plateau observed in their storage modulus (see Figure 6): while it is expected that the extremities of branches of the supramolecular polymer brushes relax and disentangle at high frequency, their core, which is formed by the aggregated ODIN groups as well as by a part of the PTHF branches (close to the ODIN), needs much longer time to relax.

The difference between **ODIN** and UPy is summarized in Figure 7, which presents the proposed morphology of (a) supramolecular bottlebrush polymers formed by the aggregation of the ODIN end-groups (localized at one chain end) and (b) polymeric assemblies formed by the aggregation of only few UPy groups (localized at one chain end). For samples **3a**−**d**, under an oscillatory shear (within the linear viscoelastic regime; see Figure 6) applied to the samples, first, the PTHF arms are expected to renew their orientations at a local level ($<M_e$) via Rouse-like motions until they reach their entanglement plateau (outside the experimental frequency window). This fast relaxation process should be followed by partial disentanglement of the chains. It has to be noted that at low temperatures, one side of the polymeric chains is fixed, which prevents the reptative motion, which is the dominant mode of stress relaxation in the linear monodisperse polymers. Therefore, disentanglement can take much longer, through contour length fluctuations (CLFs) and arm retraction processes.[51] But it stays too fast to be measured. At larger length (time) scales, the relaxed part of the polymeric brush acts as a "solvent" and the parts close to the backbone are much less constrained (moving in a dilated tube). The backbone can then explore its surrounding by Rouse motions. This mode of relaxation is also called constraint release Rouse (CRR).[51] While the CRR relaxation is not visible in the case of lower molecular weights (**3a** and **3b**), it is observed, at least

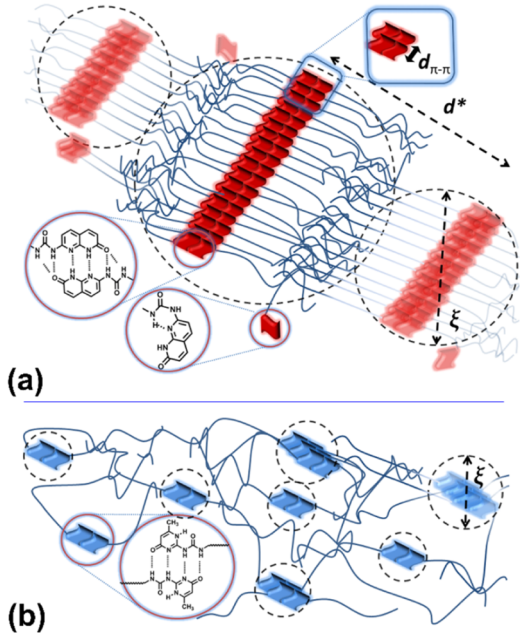

Figure 7. Tentative representation of (a) supramolecular bottlebrush polymers **3a**−**d** assuming the interaction between the cores of the supramolecular brushes is responsible for the elastic behavior and (b) supramolecular polymer **3e** bearing ureido-pyrimidinone (UPy) forming small assemblies composed of few chains, without long-range interaction. d^*, $d_{\pi-\pi}$, and ξ are the lamellar periodicity, stacking distance, and the correlation length, respectively.

partially, with the longer samples (**3c** and **3d**), due to their longer disentanglement times. Then, the low-frequency plateau appears, which is attributed to the interaction between the cores of the supramolecular assemblies, which cannot easily diffuse and relax.

At low temperature, the relaxation of the supramolecular assemblies is so slow that it could not be observed based on oscillatory shear measurements, and creep measurements should be performed to assess their viscoelastic response at much longer time. Since the terminal relaxation time is not known, we cannot clearly identify the relaxation mechanism of these large assemblies. However, it has been shown that conventional bottlebrush polymers are relaxing via reptative motion,[52] which is probably the case of samples **3a** and **3b**. On the other hand, in case of samples **3c** and **3d**, the backbones of the corresponding supramolecular brushes are so short that it is not clear if they relax as bottlebrushes or as multiarm stars.[14,15]

At higher temperatures, i.e., ≈100 °C (obtained from VT-FTIR and SAXS), the stickers start to dissociate and part of the H-bonds is lost. Consequently, the stacking and size of the backbone decrease. Therefore, the correlation between objects reduces, which enhances their mobility and a fluid response ($G' < G''$) is observed. An interesting observation is the low-frequency behavior of **3a** at 60 °C (Figure 6a). This frequency sweep in fact shows that despite the dissociation of stickers at temperatures higher than 100 °C, at longer time scales but lower temperatures, the sticker can also dissociate, leading to a terminal response ($G' < G''$). This phenomenon, however, was only captured in this specific case, but more detailed temperature and frequency scans might reveal the same behavior for the other three samples. It must also be noted that the highest temperature at which an elastic behavior is

DOI: 10.1021/acsomega.9b02126
ACS Omega 2019, 4, 16481−16492

observed increases with the length of the side chains, suggesting that the aggregation lifetime depends not only on both temperature but also on chain mobility. The consistency between the temperatures in which long-range ordering/short-range stacking disappears (75−100 °C) and the fluid response is obtained (80−120 °C) confirms that it is not the binary association between the stickers (which still exists to some extent at elevated temperatures) that controls the solidlike behavior. It is rather the long-range ordering, which are responsible for this phenomenon. Thus, in this picture, the binary associations do not play a role, since the binary association only doubles the chain length, and this does not suffice to create large objects and observe a solidlike behavior, as it was shown in the case of **3e**. In other words, a strong and long-ranged stacking is needed to produce one-dimensional objects, otherwise only small aggregates are formed, which is the case for **3e**.

CONCLUSIONS

Utilizing a newly designed hydrogen-bonding moiety (sticker), a novel approach for manufacturing bottlebrush polymers is introduced. ^{1}H NMR studies and DFT calculations showed that this sticker (**ODIN**) can form a variety of conformers and dimers; however, only one monomer and one dimer are present as the dominant forms. Moreover, these studies proved the strong tendency of **ODIN** for stack formation and sextuple H-bonding in solution. VT-FTIR and PXRD showed the stacking in the solid state.

To form supramolecular bottlebrush architecture, **ODIN** was added to one end of poly(tetrahydrofuran). The strong stickers association (H-bonding and $\pi-\pi$ stacking) can resist to the steric hindrance arising from side polymer chains. SAXS studies showed a lamellar morphology, which was more visible at lower molecular weights (higher sticker concentrations). The domain size d^* in this bottlebrush polymers increases with molecular weight, and the molecular weight dependence of d^* showed that the PTHF chains are highly stretched. The molecular order disappeared at higher temperatures close to the temperature range at which **ODIN** moiety dissociates (observed from VT-FTIR). Melt rheology showed that the polymer chains close to the supramolecular backbone (**ODIN** arrays) are highly stretched and cannot relax via reptation as one of the ends is pinned to the strongly associated **ODIN** moiety. Therefore, disentanglement can take much longer, through contour length fluctuations (CLFs) and arm retraction processes. The relaxed ends of PTHF chains eventually act as solvent to let the rest of the polymeric brush undergo Rouse-like motions (constraint release Rouse or CRR). At longer times, a second rubbery plateau appears as the signature of the interactions between the cores of the entire supramolecular bottlebrush polymers. This rigid topology is also a proof of extended conformation of supramolecular bottlebrush polymers. With an increase of temperature, viscoelastic solid behavior turns into viscoelastic liquid due to reversible depolymerization of the supramolecular backbone of the bottlebrush polymer. The transition temperature range (80−120 °C) is close to the temperature where dissociation of **ODIN** (VT-FTIR) and deformation of molecular orders (SAXS) occur (75−100 °C), which means that the stacking and size of the supramolecular backbone decreases and a fluid response ($G' < G''$) is observed.

Thus, these materials adapt their properties from viscoelastic liquids to solids and vice versa, with a modulus which makes them suitable for processing, especially that these polymers are not a transient network. In addition, they can be applied in supersoft materials as well.

Future studies focus on a detailed analysis of different chemistry, molecular weight, and topology of these novel supramolecular bottlebrush polymers to further understand the terminal relaxation mechanism of these supramolecular brush polymers. To this end, it would be helpful to perform creep measurements. Piezo-rheometry would also be useful, to visualize the first rubbery plateau, before the disentanglement of the branches.

EXPERIMENTAL SECTION

Materials. Anhydrous tetrahydrofuran (THF) (water content less than 50 ppm) was purchased from Alfa Aesar. Hexamethylene diisocyanate (HDI) was purchased from TCI. Low-molecular-weight ($M_n \approx 1$ kg mol^{-1}) dihydroxyl poly(tetrahydrofuran), acryloyl chloride, silver tetrafluoroborate ($AgBF_4$), silver hexafluorophosphate ($AgPF_6$), dibutyltin dilaurate (DBTDL), malic acid, 2,6-diaminopyridine, (anhydrous) dimethyl sulfoxide-d_6, and chloroform-d were purchased from Aldrich without further purification. 7-Amino-1,8-naphthyridin-2(1H)-one was synthesized by a previously published method.[53]

Characterization. ^{1}H NMR spectra were recorded at room temperature on a Varian VXR 400 MHz (^{1}H: 400 MHz) spectrometer using deuterated solvents. Chemical shifts (δ) are reported in ppm, whereas the chemical shifts are calibrated to the solvent residual peaks. For the self-assembly studies in solution, mixtures with different compositions of anhydrous dimethyl sulfoxide-d_6 and chloroform-d were prepared. Tetramethylsilane was used for calibration of chemical shifts. Gel permeation chromatography (GPC) measurements were performed in THF at 25 °C (1 mL min^{-1}) on a Spectra-Physics AS 1000, equipped with PLGel 5 μm × 30 cm mixed-C columns. Universal calibration was applied using a Viscotek H502 viscometer and a Shodex RI-71 refractive index detector. The GPC was calibrated using narrow-disperse polystyrene standards (Polymer Laboratories).

Melt rheology was carried out via a TA Instruments, AR 1000 under nitrogen flow, and 8 mm parallel-plate geometries and an interplate gap of 0.8−1 mm were used in all cases. Samples were vacuum-dried overnight before use. All measurements were performed in the linear viscoelastic regime, determined via torque sweep measurements. Frequency sweeps 0.01−10 Hz were carried out in different temperatures between 40 and 160 °C. The samples were prepared as follows: the bulk samples were dried in an oven at 35 °C under vacuum for 56 h. This can also anneal the samples since this temperature is found to be above the melting point of polymers. Afterward, the samples were loaded within the plate−plate geometries and were left there for 30 min at 40 °C before increasing the temperature step by step to 160 °C. The measurements at 40 °C were repeated immediately after the first round of temperature increase (up to 160 °C) and once again after 1 day. It was observed that the data are reproducible after 1 day. This in fact indicates the structure formation is lost after each heating but recovers slowly within 1 day. This is additional proof of intactness of the acrylate end-group during heating. Moreover, the GPC measurement for samples **3d** was repeated to see whether the end-group has reacted or not (Figure S14) Variable-temperature FTIR (VT-FTIR) measurements were conducted on a Bruker IFS88 FTIR spectrometer.

DOI: 10.1021/acsomega.9b02126
ACS Omega 2019, 4, 16481−16492

At each temperature, sample was left 15 min to equilibrate the temperature and then the spectrum was obtained. Differential scanning calorimetry (DSC) measurements were done on a TA Instruments Q1000. The samples were heated from room temperature to 55 °C and kept there for 15 min to remove the thermal history. Then, they were cooled down to −20 °C with a rate of 5 °C min^{-1}, equilibrated for 15 min, and heated (10 °C min^{-1}) to 160 °C. The second heating cycle was repeated to check the reproducibility of the data.

DFT. Molecular geometries and hydrogen-bonded complexes have been fully optimized using density functional theory (DFT) with the omega B97X-D functional as implemented in Q-Chem, and the basis sets were corrected.

Small-Angle X-ray Scattering (SAXS). SAXS experiments were performed at the MINA Instrument in Groningen. The MINA instrument is equipped with a rotating Cu anode operating at 45 kV and 60 mA (X-ray wavelength λ = 1.54 Å). SAXS patterns were recorded using Vantec Bruker detectors with a 10 min exposure time. The beam size on the sample was 0.25 mm. The sample temperature was controlled using a Linkam TMS600 hot stage. Two different sample-to-detector distances of 24 and 200 cm were used to cover an extended angular range. The beam center position at the detector and the exact sample-to-detector position (i.e., the scattering angles) were determined using the diffraction rings from a standard silver behenate powder. The data were radially integrated and merged into a single curve using a MATLAB code. Samples were placed into aluminum hollow disk holders (1 mm thick) sealed with kapton tape. The samples were kept for 5 h at 50 °C to make sure no crystal exists then at 25 °C annealed for 4 days. They were kept at 25 °C before starting the measurements.

Powder X-ray Diffraction (PXRD). The PXRD pattern was recorded on a Bruker D8 advanced diffractometer (Cu Kα radiation, λ = 1.54 Å) in the angular range of 5−80° (2θ) at room temperature.

Synthesis of Poly(tetrahydrofuran)s (PTHFs) 1a−d. The general procedure is as follows: a 500 mL three-neck flask equipped with an egg-shaped magnetic stirrer was dried and put under N_2 atmosphere. $AgPF_6$ (252 mg, 1 mmol) was added to 150 mL of anhydrous THF, followed by addition of 90 mg of 1 mmol acryloyl chloride at room temperature, after which a white solid arose. The mixture was left stirring to polymerize. After 3 min, 10 mL of water was added to quench the reaction. The mixture was poured into cold water. The precipitate was filtered off by using a Buchner funnel or in the case of lower molecular weights using centrifugation at 5 °C (4500 rpm). The oil was dissolved in 250 mL of diethyl ether. The ether solution was washed with 250 mL of ammonium hydroxide and 100 mL of brine. The organic fraction was dried over magnesium sulfate, filtered, and the solvent was removed under reduced pressure. A white solid of **1** was obtained.

Yield: 2.8 g. ^{1}H NMR (400 MHz, chloroform-*d*) δ: 6.37 (d, $1H_1$), 6.10 (dd, $1H_2$), 5.76 (d, $1H_3$), 4.17 (t, $2H_4$), 3.63 (t, $2H_5$), 3.42 (brs, $412H_6$), 1.61 (brs, $444H_7$).

Synthesis of 1-(6-Isocyanatohexyl)-3-(7-oxo-7,8-dihydro-1,8-naphthyridin-2-yl)urea 2 (ODIN). 7-Amino-1,8-naphthyridin-2(1*H*)-one (4 g, 0.025 mol) was added to a 100 mL three-neck round-bottom flask equipped with an egg-shaped magnetic stirrer. The solids were allowed to dry for 1 h under vacuum. The flask was kept under nitrogen atmosphere by three consequent vacuum/nitrogen cycles. HDI (60 mL, 0.37 mol) was added to the reaction flask. The reaction mixture was heated to 110 °C while stirring. After 19 h, the reaction mixture was cooled down to room temperature. Then, it was precipitated in 500 mL of hexane. The precipitate was filtered off and the traces of HDI were removed by distillation under reduced pressure (0.01 mbar) at 130 °C. (84% yield)

^{1}H NMR (400 MHz, DMSO-d_6) δ: 12.15 (s, $1H_1$), 9.63 (s, $1H_2$), 8.98 (t, $1H_7$), 7.88 (d, J = 8.5 Hz, $1H_4$), 7.75 (d, J = 9.4 Hz, $1H_5$), 6.83 (d, J = 8.5 Hz, $1H_3$), 6.31 (dd, J = 9.3, 1.9 Hz, $1H_6$), 3−3.3 (m, $4H_8$), 1.1−1.6 (m, $8H_9$).

^{1}H NMR (400 MHz, chloroform-*d*) δ: 12.75 (s, $1H_1$), 11.22 (s, $1H_2$), 8.19 (d, J = 8.8 Hz, $1H_3$), 7.80 (d, J = 8.8 Hz, $1H_4$), 7.70 (d, J = 9.3 Hz, $1H_5$), 6.45 (d, J = 9.3 Hz, $1H_6$), 5.93 (s, $1H_7$), 3.05−3.45 (m, $4H_8$), 1.25−1.75 (m, $8H_9$).

Synthesis of 1-(6-Isocyanatohexyl)-3-(7-oxo-7,8-dihydro-1,8-naphthyridin-2-yl)urea-PTHF (3a−d). A 100 mL three-neck round-bottom flask was equipped with a reflux condenser with an egg-shaped magnetic stirrer and put under nitrogen atmosphere. Poly(tetrahydrofuran) acrylate (PTHF-acrylate, 300 mg) and 3 equiv of isocyanate **2** were added to the reaction flask under nitrogen atmosphere. Then, 20 mL of anhydrous chloroform and two droplets of DBTDL were added to the reaction mixture. The reaction mixture was refluxed overnight, and then, the solvent was removed under reduced pressure. The polymer was isolated by dissolving the solid into ethyl acetate and transferring it to a centrifuge tube, which was centrifuged at 4500 rpm at 0 °C for 30 min. The unreacted isocyanate **2** precipitates at the bottom of the tube. The solution was collected, and the solvent was removed under reduced pressure. A yellow solid was obtained (conversion = 70−85%).

^{1}H NMR (400 MHz, chloroform-*d*) δ: 12.84 (s, $1H_1$), 11.22 (s, $1H_2$), 8.21 (d, $1H_3$), 7.80 (d, J = 8.6 Hz, $1H_4$), 7.70 (d, J = 9.4 Hz, $1H_5$), 6.49 (d, J = 9.5 Hz, $1H_6$), 6.36 (dd, J = 17.4, 1.5 Hz, $1H_7$), 6.09 (dd, J = 17.3, 10.4 Hz, $1H_8$), 6.01 (s, $1H_9$), 5.78 (dd, J = 10.4, 1.5 Hz, $1H_{10}$), 4.76 (s, $1H_{11}$), 4.16 (t, J = 6.6 Hz, $2H_{12}$), 4.03 (t, $2H_{13}$), 3.40 (brs, $378H_{14}$), 3.14 (t, $4H_{15}$), 1.63 (brs, $404H_{16,17}$).

Synthesis of PTHF-UPy (3e). The synthesis was similar to **3a−d**, except that chloroform was used in centrifugation.

^{1}H NMR (400 MHz, chloroform-*d*) δ: 13.11 (s, $1H_1$), 11.83 (s, $1H_2$), 10.10 (d, $1H_3$), 6.36 (dd, J = 17.4, 1.5 Hz, $1H_4$), 6.11 (dd, J = 17.3, 10.4 Hz, $1H_5$), 5.84 (s, $1H_6$), 5.81 (dd, J = 10.5, 1.5 Hz, $1H_7$), 5.10 (s, $1H_8$), 4.16 (t, J = 6.6 Hz, $2H_9$), 4.03 (t, $2H_{10}$), 3.40 (m, H_{11}), 3.14 (t, $4H_{12}$), 3.00−3.50 (m, $H_{13,14}$), 2.15 (s, $3H_{15}$), 1.30−1.63 (m, $H_{16,17}$) (conversion = 65−84%).

Calculation of K_{dim}. As the **ODIN** dimer and monomer are in slow exchange on the ^{1}H NMR timescale, it is possible to calculate the molar concentration of monomer and dimer based on the integrals of the NMR signals, the ratio of which is defined as $y = (I_{mon}/I_{dim})$. From this ratio and the overall **ODIN** concentration (U_0), the dimerization constant (K_{dim}) can be calculated using the following equation

$$K_{dim} = \frac{y(y+1)}{2U_0}$$

■ ASSOCIATED CONTENT

Supporting Information

The Supporting Information is available free of charge on the ACS Publications website at DOI: 10.1021/acsomega.9b02126.

DOI: 10.1021/acsomega.9b02126
ACS Omega 2019, 4, 16481−16492

GPC traces, ^{1}H NMR spectra of **1** and **2**, optimized geometries, full frequency sweeps for **3c** and **3d**, and DSC curves (PDF)

AUTHOR INFORMATION

Corresponding Author

*E-mail: k.u.loos@rug.nl. Tel: +31-50 363 6867.

ORCID

Csaba Fodor: 0000-0002-5157-0535

Evelyne van Ruymbeke: 0000-0001-7633-0194

Giuseppe Portale: 0000-0002-4903-3159

Katja Loos: 0000-0002-4613-1159

Present Address

[‖]Department of Chemistry, University of Basel, Mattenstrasse 24a, BPR1096, 4002 Basel, Basel-Stadt, Switzerland (C.F.).

Author Contributions

The manuscript was written through contributions of all authors.

Funding

The research was supported by an NWO-VICI innovational research grant.

Notes

The authors declare no competing financial interest.

ACKNOWLEDGMENTS

The authors are grateful to A.J.J. Woortman (RUG) for GPC measurements, Dr. A. Vagias (RUG) for fruitful discussions, and Judit Schöbel for assisting in the graphic designs. Evelyne van Ruymbeke is research associate of FNRS.

REFERENCES

(1) Kapnistos, M.; Vlassopoulos, D.; Roovers, J.; Leal, L. G. Linear Rheology of Architecturally Complex Macromolecules: Comb Polymers with Linear Backbones. *Macromolecules* **2005**, *38*, 7852−7862.

(2) van Ruymbeke, E.; Bailly, C.; Keunings, R.; Vlassopoulos, D. A General Methodology to Predict the Linear Rheology of Branched Polymers. *Macromolecules* **2006**, *39*, 6248−6259.

(3) Gury, L.; Gauthier, M.; Cloitre, M.; Vlassopoulos, D. Colloidal Jamming in Multiarm Star Polymer Melts. *Macromolecules* **2019**, *52*, 4617−4623.

(4) van Ruymbeke, E.; Vlassopoulos, D.; Mierzwa, M.; Pakula, T.; Charalabidis, D.; Pitsikalis, M.; Hadjichristidis, N. Rheology and Structure of Entangled Telechelic Linear and Star Polyisoprene Melts. *Macromolecules* **2010**, *43*, 4401−4411.

(5) Daniels, D. R.; McLeish, T. C. B.; Kant, R.; Crosby, B. J.; Young, R. N.; Pryke, A.; Allgaier, J.; Groves, D. J.; Hawkins, R. J. Linear rheology of diluted linear, star and model long chain branched polymer melts. *Rheol. Acta* **2001**, *40*, 403−415.

(6) Daniels, D. R.; McLeish, T. C. B.; Crosby, B. J.; Young, R. N.; Fernyhough, C. M. Molecular Rheology of Comb Polymer Melts. 1. Linear Viscoelastic Response. *Macromolecules* **2001**, *34*, 7025−7033.

(7) Milner, S. T.; McLeish, T. C. B. Arm-Length Dependence of Stress Relaxation in Star Polymer Melts. *Macromolecules* **1998**, *31*, 7479−7482.

(8) Milner, S. T.; McLeish, T. C. B.; Young, R. N.; Hakiki, A.; Johnson, J. M. Dynamic Dilution, Constraint-Release, and Star−Linear Blends. *Macromolecules* **1998**, *31*, 9345−9353.

(9) McLeish, T. C. B. Molecular rheology of H-polymers. *Macromolecules* **1988**, *21*, 1062−1070.

(10) Inkson, N. J.; Graham, R. S.; McLeish, T. C. B.; Groves, D. J.; Fernyhough, C. M. Viscoelasticity of Monodisperse Comb Polymer Melts. *Macromolecules* **2006**, *39*, 4217−4227.

(11) Park, S. J.; Shanbhag, S.; Larson, R. G. A hierarchical algorithm for predicting the linear viscoelastic properties of polymer melts with long-chain branching. *Rheol. Acta* **2005**, *44*, 319−330.

(12) Larson, R. G. Combinatorial Rheology of Branched Polymer Melts. *Macromolecules* **2001**, *34*, 4556−4571.

(13) Lee, J. H.; Fetters, L. J.; Archer, L. A. Stress Relaxation of Branched Polymers. *Macromolecules* **2005**, *38*, 10763−10771.

(14) Pakula, T.; Vlassopoulos, D.; Fytas, G.; Roovers, J. Structure and Dynamics of Melts of Multiarm Polymer Stars. *Macromolecules* **1998**, *31*, 8931−8940.

(15) Johnson, K. J.; Glynos, E.; Sakellariou, G.; Green, P. Dynamics of Star-Shaped Polystyrene Molecules: From Arm Retraction to Cooperativity. *Macromolecules* **2016**, *49*, 5669−5676.

(16) Doi, M.; Edwards, S. F. *The Theory of Polymer Dynamics*, 1st ed.; Clarendon Press: Oxford, 1988; pp 1−391.

(17) Allgaier, J.; Hövelmann, C. H.; Wei, Z.; Staropoli, M.; Pyckhout-Hintzen, W.; Lühmann, N.; Willbold, S. Synthesis and rheological behavior of poly(1,2-butylene oxide) based supramolecular architectures. *RSC Adv.* **2016**, *6*, 6093−6106.

(18) Staropoli, M.; Raba, A.; Hövelmann, C. H.; Appavou, M.-S.; Allgaier, J.; Krutyeva, M.; Pyckhout-Hintzen, W.; Wischnewski, A.; Richter, D. Melt dynamics of supramolecular comb polymers: Viscoelastic and dielectric response. *J. Rheol.* **2017**, *61*, 1185−1196.

(19) Staropoli, M.; Raba, A.; Hövelmann, C. H.; Krutyeva, M.; Allgaier, J.; Appavou, M.-S.; Keiderling, U.; Stadler, F. J.; Pyckhout-Hintzen, W.; Wischnewski, A.; Richter, D. Hydrogen Bonding in a Reversible Comb Polymer Architecture: A Microscopic and Macroscopic Investigation. *Macromolecules* **2016**, *49*, 5692−5703.

(20) Golkaram, M.; Fodor, C.; van Ruymbeke, E.; Loos, K. Linear Viscoelasticity of Weakly Hydrogen-Bonded Polymers near and below the Sol−Gel Transition. *Macromolecules* **2018**, *51*, 4910−4916.

(21) Aharoni, S. M. On entanglements of flexible and rodlike polymers. *Macromolecules* **1983**, *16*, 1722−1728.

(22) Sivakova, S.; Bohnsack, D. A.; Mackay, M. E.; Suwanmala, P.; Rowan, S. J. Utilization of a Combination of Weak Hydrogen-Bonding Interactions and Phase Segregation to Yield Highly Thermosensitive Supramolecular Polymers. *J. Am. Chem. Soc.* **2005**, *127*, 18202−18211.

(23) Kumpfer, J. R.; Wie, J. J.; Swanson, J. P.; Beyer, F. L.; Mackay, M. E.; Rowan, S. J. Influence of Metal Ion and Polymer Core on the Melt Rheology of Metallosupramolecular Films. *Macromolecules* **2012**, *45*, 473−480.

(24) Burattini, S.; Greenland, B. W.; Merino, D. H.; Weng, W.; Seppala, J.; Colquhoun, H. M.; Hayes, W.; Mackay, M. E.; Hamley, I. W.; Rowan, S. J. A Healable Supramolecular Polymer Blend Based on Aromatic $\pi-\pi$ Stacking and Hydrogen-Bonding Interactions. *J. Am. Chem. Soc.* **2010**, *132*, 12051−12058.

(25) Burgess, F. J.; Cunliffe, A. V.; Richards, D. H.; Thompson, D. Organic halides as cationic initiators. *Polymer* **1978**, *19*, 334−340.

(26) Cunliffe, A. V.; Hartley, D. B.; Kingston, S. B.; Richards, D. H.; Thompson, D. Reactions of living polytetrahydrofuran with amines: 1. Pyridine. *Polymer* **1981**, *22*, 101−107.

(27) Croucher, T. G.; Wetton, R. E. Synthesis of narrow distribution polytetrahydrofuran. *Polymer* **1976**, *17*, 205−211.

(28) Fodor, C.; Kali, G.; Iván, B. Poly(N-vinylimidazole)-l-Poly(tetrahydrofuran) Amphiphilic Conetworks and Gels: Synthesis, Characterization, Thermal and Swelling Behavior. *Macromolecules* **2011**, *44*, 4496−4502.

(29) Herbst, F.; Schröter, K.; Gunkel, I.; Gröger, S.; Thurn-Albrecht, T.; Balbach, J.; Binder, W. H. Aggregation and Chain Dynamics in Supramolecular Polymers by Dynamic Rheology: Cluster Formation and Self-Aggregation. *Macromolecules* **2010**, *43*, 10006−10016.

(30) Appel, W. P. J.; Portale, G.; Wisse, E.; Dankers, P. Y. W.; Meijer, E. W. Aggregation of Ureido-Pyrimidinone Supramolecular Thermoplastic Elastomers into Nanofibers: A Kinetic Analysis. *Macromolecules* **2011**, *44*, 6776−6784.

(31) Corbin, P. S.; Zimmerman, S. C. Self-Association without Regard to Prototropy. A Heterocycle That Forms Extremely Stable

DOI: 10.1021/acsomega.9b02126
ACS Omega 2019, 4, 16481−16492

Quadruply Hydrogen-Bonded Dimers. *J. Am. Chem. Soc.* **1998**, *120*, 9710−9711.
(32) Pellizzaro, M. L.; Barrett, S. A.; Fisher, J.; Wilson, A. J. Design, synthesis and binding studies of a novel quadruple ADDA hydrogen-bond array. *Org. Biomol. Chem.* **2012**, *10*, 4899−4906.
(33) Corbin, P. S.; Zimmerman, S. C.; Thiessen, P. A.; Hawryluk, N. A.; Murray, T. J. Complexation-Induced Unfolding of Heterocyclic Ureas. Simple Foldamers Equilibrate with Multiply Hydrogen-Bonded Sheetlike Structures. *J. Am. Chem. Soc.* **2001**, *123*, 10475−10488.
(34) Ośmiałowski, B.; Mroczyńska, K.; Kolehmainen, E.; Kowalska, M.; Valkonen, A.; Pietrzak, M.; Rissanen, K. Association of N-(Pyridin-2-yl),N'-substituted Ureas with 2-Amino-1,8-naphthyridines and Benzoates: NMR and Quantum Chemical Studies of the Substituent Effect on Complexation. *J. Org. Chem.* **2013**, *78*, 7582−7593.
(35) Bailey, A.; Horton, P.; Grossel, M. Self-assembly into infinite tapes by 2,7-disubstituted-1,8-naphthyridines in the solid state. *CrystEngComm* **2010**, *12*, 4074−4079.
(36) Ośmiałowskii, B.; Kolehmainen, E.; Kalenius, E.; Behera, B.; Kauppinen, R.; Sievänen, E. Intermolecular steric hindrance in 7-acylamino-[1H]-2-oxo-1,8-naphthyridines: NMR, ESI-MS, IR, and DFT calculation studies. *Struct. Chem.* **2011**, *22*, 1143−1151.
(37) Appel, W. P. J.; Nieuwenhuizen, M.; Lutz, M.; de Waal, B.; Palmans, A.; Meijer, E. W. Supramolecular chemistry with ureido-benzoic acids. *Chem. Sci.* **2014**, *5*, 3735−3745.
(38) Abraham, R.; Byrne, J.; Griffiths, L.; Perez, M. ^{1}H chemical shifts in NMR: Part 23, the effect of dimethyl sulphoxide versus chloroform solvent on ^{1}H chemical shifts. *Magn. Reson. Chem.* **2006**, *44*, 491−509.
(39) Schneider, H. J. Binding Mechanisms in Supramolecular Complexes. *Angew. Chem., Int. Ed.* **2009**, *48*, 3924−3977.
(40) Jorgensen, W. L.; Pranata, J. Importance of secondary interactions in triply hydrogen bonded complexes: Guanine-cytosine vs uracil-2,6-diaminopyridine. *J. Am. Chem. Soc.* **1990**, *112*, 2008−2010.
(41) Ośmiałowski, B.; Kolehmainen, E.; Dobosz, R.; Gawinecki, R.; Kauppinen, R.; Valkonen, A.; Koivukorpi, J.; Rissanen, K. Self-organization of 2-acylaminopyridines in the solid state and in solution. *J. Phys. Chem. A* **2010**, *114*, 10421−10426.
(42) Etter, M. C. Encoding and decoding hydrogen-bond patterns of organic compounds. *Acc. Chem. Res.* **1990**, *23*, 120−126.
(43) De Greef, T. F. A.; Kade, M. J.; Feldman, K. E.; Kramer, E. J.; Hawker, C. J.; Meijer, E. W. Spacer-length-dependent association in polymers with multiple-hydrogen-bonded end groups. *J. Polym. Sci., Part A: Polym. Chem.* **2011**, *49*, 4253−4260.
(44) Tellers, J.; Canossa, S.; Pinalli, R.; Soliman, M.; Vachon, J.; Dalcanale, E. Dynamic Cross-Linking of Polyethylene via Sextuple Hydrogen Bonding Array. *Macromolecules* **2018**, *51*, 7680−7691.
(45) Guo, D.; Sijbesma, P. R.; Zuilhof, H. π-Stacked Quadruply Hydrogen-Bonded Dimers: π-Stacking Influences H-Bonding. *Org. Lett.* **2004**, *6*, 3667−3670.
(46) Zhou, T.; Li, F.; Fan, Y.; Song, W.; Mu, X.; Zhang, H.; Wang, Y. Hydrogen-bonded dimer stacking induced emission of amino-benzoic acid compounds. *Chem. Commun.* **2009**, 3199−3201.
(47) Mroczyńska, K.; Kaczorowska, M.; Kolehmainen, E.; et al. Conformational equilibrium in supramolecular chemistry: Dibutyl-triuret case. Beilstein. *J. Org. Chem.* **2015**, *11*, 2105−2116.
(48) Luo; Wang, J.; Ying. Hydrogen-Bonding Properties of Segmented Polyether Poly(urethane urea) Copolymer. *Macromolecules* **1997**, *30*, 4405−4409.
(49) He, Y.; Xie, D.; Zhang, X. The structure, microphase-separated morphology, and property of polyurethanes and polyureas. *J. Mater. Sci.* **2014**, *49*, 7339−7352.
(50) Mattia, J.; Painter, P. A Comparison of Hydrogen Bonding and Order in a Polyurethane and Poly(urethane−urea) and Their Blends with Poly(ethylene glycol). *Macromolecules* **2007**, *40*, 1546−1554.
(51) Hawke, L. G. D.; Ahmadi, M.; Goldansaz, H.; van Ruymbeke, E. Viscoelastic properties of linear associating poly(n-butyl acrylate) chains. *J. Rheol.* **2016**, *60*, 297−310.
(52) Vlassopoulos, D.; Stiakakis, E.; Kapnistos, M. Model Soft Colloids Out of Equllibrium Glass-like and Re-entrant Transitions. *Rheol. Rev.* **2007**, 179−252.
(53) Newkome, G. R.; Garbis, S. J.; Majestic, V. K.; Fronczek, F. R.; Chiari, G. Chemistry of heterocyclic compounds. 61. Synthesis and conformational studies of macrocycles possessing 1,8- or 1,5-naphthyridino subunits connected by carbon-oxygen bridges. *J. Org. Chem.* **1981**, *46*, 833−839.

DOI: 10.1021/acsomega.9b02126
ACS Omega 2019, 4, 16481−16492